AMERICAN SOCIETY FOR MICROBIOLOGY | Journal of Virology®

VIRUS-CELL INTERACTIONS

Membrane Protein of Human Coronavirus NL63 Is Responsible for Interaction with the Adhesion Receptor

Antonina Naskalska,[a,b] Agnieszka Dabrowska,[a,b] Artur Szczepanski,[a,b] Aleksandra Milewska,[a,b] Krzysztof Piotr Jasik,[c] Krzysztof Pyrc[a]

[a]Virogenetics Laboratory of Virology, Malopolska Centre of Biotechnology, Jagiellonian University, Krakow, Poland
[b]Microbiology Department, Faculty of Biochemistry, Biophysics, and Biotechnology, Jagiellonian University, Krakow, Poland
[c]School of Pharmacy, Division of Laboratory Medicine, Medical University of Silesia in Katowice, Sosnowiec, Poland

ABSTRACT Human coronavirus NL63 (HCoV-NL63) is a common respiratory virus that causes moderately severe infections. We have previously shown that the virus uses heparan sulfate proteoglycans (HSPGs) as the initial attachment factors, facilitating viral entry into the cell. In the present study, we show that the membrane protein (M) of HCoV-NL63 mediates this attachment. Using viruslike particles lacking the spike (S) protein, we demonstrate that binding to the cell is not S protein dependent. Furthermore, we mapped the M protein site responsible for the interaction with HSPG and confirmed its relevance using a viable virus. Importantly, *in silico* analysis of the region responsible for HSPG binding in different clinical isolates and the Amsterdam I strain did not exhibit any signs of cell culture adaptation.

IMPORTANCE It is generally accepted that the coronaviral S protein is responsible for viral interaction with a cellular receptor. Here we show that the M protein is also an important player during early stages of HCoV-NL63 infection and that the concerted action of the two proteins (M and S) is a prerequisite for effective infection. We believe that this study broadens the understanding of HCoV-NL63 biology and may also alter the way in which we perceive the first steps of cell infection with the virus. The data presented here may also be important for future research into vaccine or drug development.

KEYWORDS HCoV-NL63, attachment, heparan sulfate proteoglycans, membrane protein, viruslike particles

Receptor recognition by viruses is the first and essential step of viral infection. Understanding this process can provide critical insight into viral biology and, ultimately, the development of effective vaccines and antivirals.

Coronaviruses (CoVs), enveloped RNA viruses, infect a wide variety of species, causing various clinical conditions. The tissue and species specificities are determined by the presence of appropriate adhesion and entry receptors on the cell surface. Some alphacoronaviruses, e.g., transmissible gastroenteritis coronavirus (TGEV) and feline infectious peritonitis coronavirus (FIPV), employ aminopeptidase N, whereas human coronavirus NL63 (HCoV-NL63) utilizes angiotensin-converting enzyme 2 (ACE2) (1–3). At the same time, ACE2 serves as a receptor for severe acute respiratory syndrome coronavirus (SARS-CoV), a betacoronavirus (4). A number of receptors have been described for betacoronaviruses, including carcinoembryonic antigen-related cell adhesion molecule 1 for murine hepatitis virus (MHV), dipeptidyl peptidase 4 for Middle East respiratory syndrome coronavirus (MERS-CoV), and major histocompatibility complex class I for human coronavirus OC43 (5–9). Furthermore, several alpha-, beta-, and gammacoronaviruses, e.g., TGEV, human coronavirus HKU1, HCoV-OC43, bovine respiratory coro-

Citation Naskalska A, Dabrowska A, Szczepanski A, Milewska A, Jasik KP, Pyrc K. 2019. Membrane protein of human coronavirus NL63 is responsible for interaction with the adhesion receptor. J Virol 93:e00355-19. https://doi.org/10.1128/JVI.00355-19.

Editor Tom Gallagher, Loyola University Chicago

Address correspondence to Antonina Naskalska, antonina.naskalska@uj.edu.pl, or Krzysztof Pyrc, k.a.pyrc@uj.edu.pl.

Received 28 February 2019
Accepted 12 July 2019
Accepted manuscript posted online 17 July 2019
Published 12 September 2019

navirus (BCoV), and avian infectious bronchitis virus (IBV), reportedly use sialic acids for initial attachment to the cell (summarized in reference 10).

The coronaviral particle consists of a dense core formed by a nucleocapsid (N) protein with viral genomic RNA and an envelope decorated with the membrane (M), envelope (E), and spike (S) proteins. Some coronaviruses contain other structural proteins, such as hemagglutinin esterase (HE) or accessory open reading frame (ORF) proteins (ORF3, ORF4a, and ORF7) (59, 69). The S protein is a class I viral membrane glycoprotein responsible for the interaction with the entry receptor and fusion (11).

HCoV-NL63 employs ACE2 as an entry receptor (3). However, we recently reported that heparan sulfate (HS) proteoglycans (HSPGs) are required for effective adhesion of the virus to the cell surface and that such an interaction enhances the infection process (12). HSPG binding was also demonstrated for MHV (13), SARS-CoV (14), and porcine epidemic diarrhea virus (PEDV) (15).

HSPGs are glycoproteins that are ubiquitous at the surface of the mammalian cell. Binding to HSPG is the initial event promoting subsequent recognition of a secondary receptor by increasing the local concentration of pathogens or triggering conformational changes of proteins involved in viral entry. As an example, binding to HSPG induces structural rearrangements of proteins responsible for infection by adeno-associated virus 2 (16), adenovirus types 2 and 5 (17), human papillomavirus 16 (18), and several herpesviruses (19). Furthermore, the majority of oncogenic viruses (hepatitis B and C viruses, Kaposi's sarcoma-associated herpesvirus, human papillomaviruses, Merkel cell polyomavirus, and human T cell lymphotropic virus type 1) initially attach to the HSPGs (20). HSPGs can also enhance virulence by binding accessory viral factors necessary for viral replication. This is illustrated by HSPG binding of the Tat protein of human immunodeficiency virus, which after internalization activates transcription of the viral RNA (21).

To better address the nature of the virus-HSPG interaction, we constructed viruslike particles (VLPs) composed of HCoV-NL63 proteins. VLPs structurally mimic the native virus and thus constitute a good model for studying virus-host interactions in the context of additional capsid components. Importantly, VLPs can be relatively easily tailored by molecular biotechnology techniques, facilitating the assessment of the role of individual viral proteins in receptor recognition.

In the present study, we demonstrate that HCoV-NL63 binds HSPG via the M protein, which is to some extent responsible for virus attachment. We thus show that viral entry is an outcome of the concerted action of the M and S proteins. The presented findings improve the understanding of viral biology and may facilitate the development of improved antivirals and neutralizing vaccines.

RESULTS

Production and purification of VLPs. HCoV-NL63 VLPs composed of the M, E, N, and (optionally) S proteins were produced in insect cells, as previously described (22), with the modification that the N protein was also included. To evaluate protein expression, insect cells infected with bicistronic recombinant baculovirus (rBV) coding for M and E proteins (M+E) and monocistronic N rBV (and optionally monocistronic S rBV) were immunostained and examined under a confocal microscope. Colocalization of the M and N proteins was observed, suggesting the formation of a protein complex within the producer cells (Fig. 1A). To verify whether VLPs were effectively assembled and released, the culture medium harvested from insect cells expressing M, E, N, and S proteins was analyzed by Western blotting. The M (26-kDa), N (42-kDa), and S (150-kDa) proteins were detected in the secreted fraction when insect cells were coinfected with (M+E) rBV, N rBV, and, optionally, S rBV (Fig. 1B). In agreement with our previous studies, the M protein migrated as two bands, reflecting its two different glycosylation states. Similarly, two bands of the N protein were observed, upon electrophoresis, resulting from protein degradation under denaturing conditions (23). In contrast, the apparent molecular weight of the S protein band was higher than expected, most likely because of the glycosylation and/or incomplete denaturation of the protein trimer. Both VLPs, composed of M, E, and N (MEN) and M, E, N, and

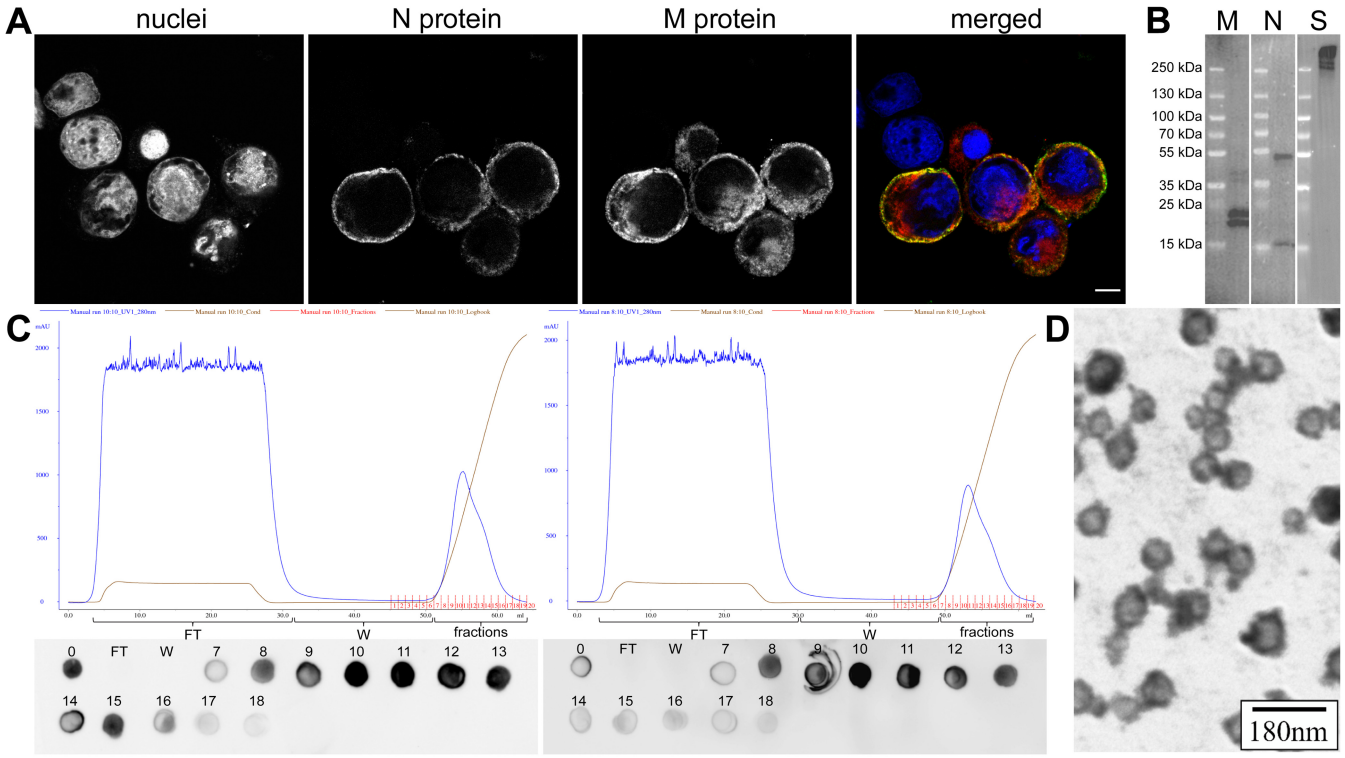

FIG 1 Production of HCoV-NL63 VLPs. (A) Fluorescence microscope images of insect cells expressing N and M proteins. N protein was detected with mouse monoclonal antibody and is immunostained in green, whereas M protein was detected with rabbit polyclonal serum and is immunostained in red. Cell nuclei are immunostained with DAPI. Bar = 10 μm. (B) As anti-S antibody could not be used for immunostaining, S protein incorporation was demonstrated by Western blotting. Culture medium was harvested from insect cells infected with (M+E) rBV, N rBV, and S rBV. M, N, and S are lanes from blots detected with anti-M, anti-N, and anti-S antibodies, respectively. (C) Purification profiles of MEN and MENS VLPs on a heparin column. Collected fractions were analyzed by dot blotting with anti-M antibody. Numbers correspond to eluted fractions numbered on the chromatogram. "0," sample prior purification; FT, flowthrough fraction; W, wash fraction. (D) TEM image of purified and positively stained MENS VLPs.

S (MENS) proteins, were concentrated and purified using a heparin column according to a previously developed protocol (22) (Fig. 1C). The analysis of purified samples by transmission electron microscopy (TEM) showed spherical particles of different diameters, which might reflect the amount of the N protein incorporated into VLPs (Fig. 1D).

Spike protein is dispensable for HCoV-NL63 VLP adhesion to LLC-Mk2 cells. Previously, we have shown that HCoV-NL63 VLPs composed of the M, E, and S proteins penetrate LLC-Mk2 cells, which are naturally permissive to HCoV-NL63 infection, and that this process is ACE2 dependent. We have also observed that VLPs composed of M and E proteins adhere to but do not enter the target cell (data not shown). In the present study, we evaluated the binding and endocytosis of MEN and MENS HCoV-NL63 VLPs.

LLC-Mk2 cells were incubated with the purified MEN and MENS VLPs, and we found that MEN VLPs localize to the cell surface, whereas MENS VLPs were present on the cell surface and in the cytoplasm (Fig. 2). This confirmed that the S protein is required for particle internalization but dispensable for VLP adhesion. To further validate this result, we blocked the virus-ACE2 interaction with anti-ACE2 antibody, which resulted in inhibition of MENS VLP internalization but not adhesion to the cell surface (Fig. 3). Interestingly, for MENS VLPs, we observed a higher number of viral particles on cells preincubated with anti-ACE2 antibodies. We believe that this is an artifact, as during entry, VLPs fuse with cellular membranes, which results in diffusion of the fluorescence signal and a decrease of the score. Blocking of the interaction with the cellular receptor hampers VLP-cell fusion, and the scored number of particles remains high. Adhesion of MEN VLPs to cells was not affected by inhibition of the VLP-ACE2 interaction. Altogether, these observations indicate that S protein of HCoV-NL63 is not involved in virus attachment to target cells.

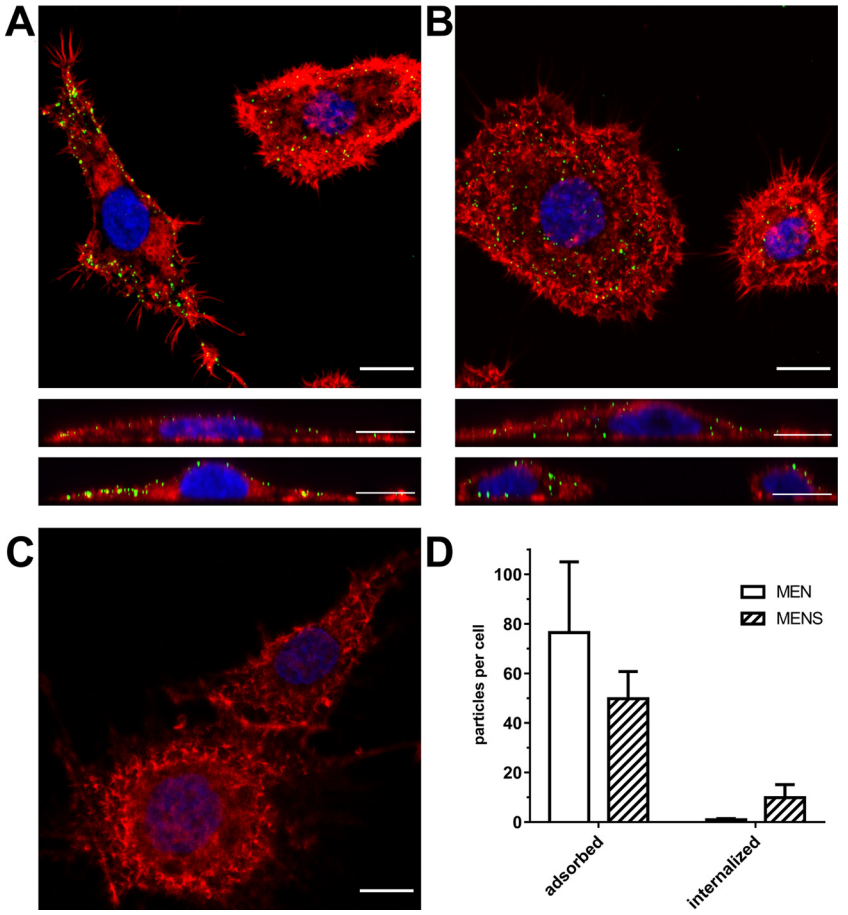

FIG 2 MEN VLP and MENS VLP adhesion to and internalization in susceptible cells. (A to C) Confocal microscopy images of LLC-Mk2 cells incubated with purified MEN VLPs (A) and MENS VLPs (B) and mock-incubated control cells (C). The bottom lanes of panels A and B show the *xz* plane in orthogonal views. VLPs were detected with anti-M polyclonal serum and are immunostained in green, actin fibers were immunostained with phalloidin and are shown in red, and nuclei were immunostained with DAPI and are shown in blue. Bars = 10 μm. (D) Graph showing quantification of the adsorbed and internalized VLPs. Data are presented as means ± standard deviations (SD). Each bar shows data from a minimum of 24 106- by 106-μm fields of view, registered from three different samples.

MEN and MENS VLPs use heparan sulfate as an adhesion receptor. Using flow cytometry, we next investigated whether the adhesion of MEN and MENS VLPs to the cell surface involves interaction with HSPGs, as has been shown for HCoV-NL63. For this, purified VLPs were preincubated with soluble HS and used to inoculate LLC-Mk2 cells. Identical samples were prepared using untreated VLPs. The cells were then immunostained to label the VLPs, and the signal was recorded. Native, iodixanol-concentrated HCoV-NL63 was used as a control. We observed that both MEN and MENS VLPs bound to the cell surface in the absence of HS and that HS pretreatment of VLPs hampered adhesion (Fig. 4).

Peptides of the membrane protein are recognized by heparin. MEN VLPs contain the N protein encapsulated in an envelope formed by the M and E proteins. We have *a priori* assumed that the M protein serves as a partner for cellular HSPG during viral or VLP adhesion, and we verified this hypothesis experimentally. First, an array of synthetic, overlapping peptides covering the complete M protein was used to test binding with the labeled heparin. The M protein regions potentially interacting with heparin were hence identified as amino acids (aa) 25 to 51, aa 93 to 119, and aa 153 to 207 (Fig. 5). Most of the peptides are arginine and lysine rich, which is in agreement with previously reported data (24, 25).

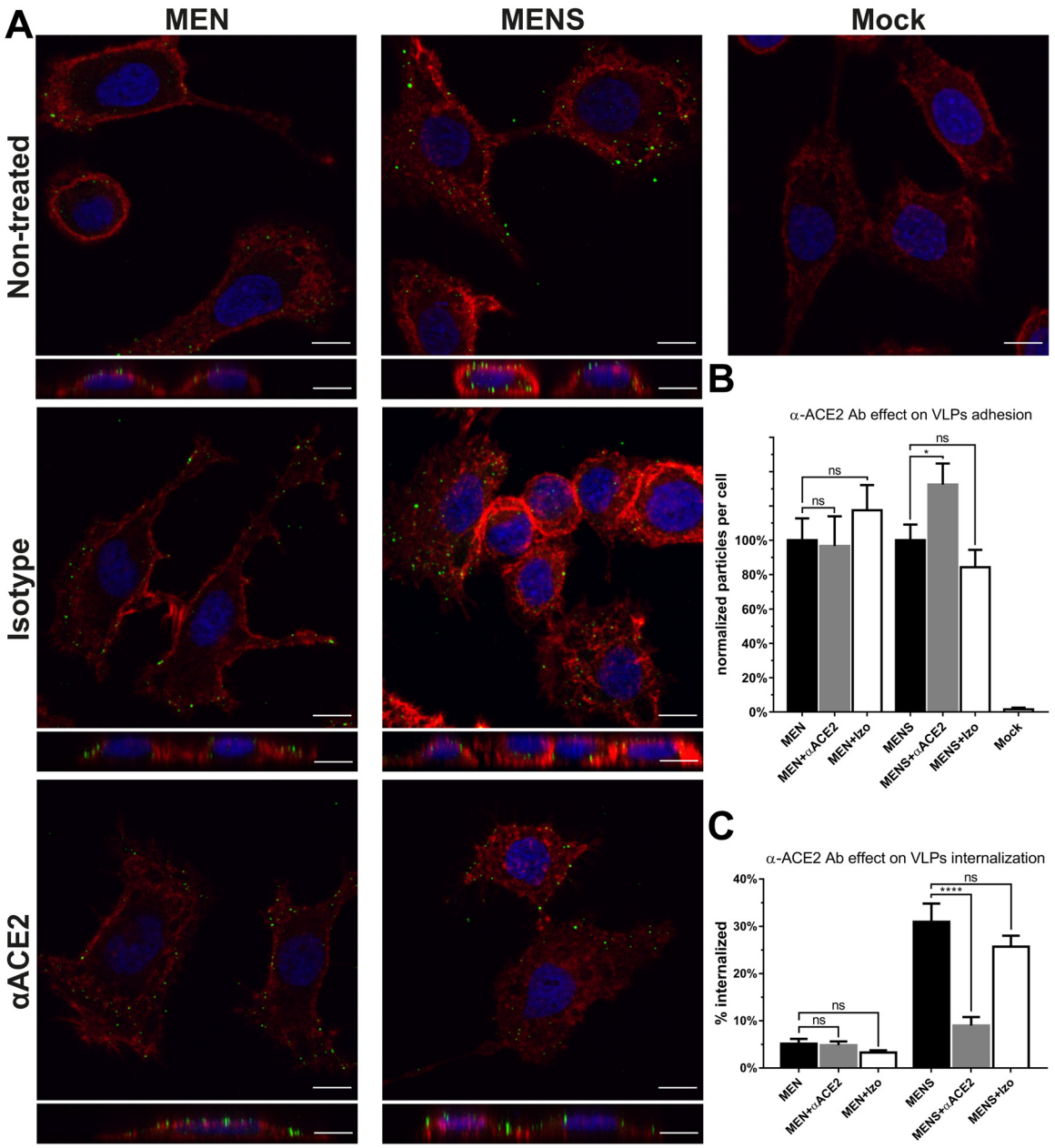

FIG 3 Adhesion and internalization of MEN and MENS VLPs in the presence of anti-ACE2 antibodies. (A) Cells preincubated with anti-ACE antibody (denoted αACE) or isotype antibody control (denoted Izo) were incubated with purified MEN or MENS VLPs. VLPs were detected with anti-M polyclonal serum and are immunostained in green, actin fibers were stained with phalloidin and are shown in red, and nuclei were stained with DAPI and are shown in blue. The bottom lanes show the *xz* plane in orthogonal views. Bars = 10 μm. (B) Graph showing the total number of VLPs per cell. Data were normalized to the values for untreated control samples (MEN and MENS. (C) Graph showing the proportion of VLPs inside the cell compared to the total number of VLPs observed on the cell. Each bar on graphs shows data from a minimum of 60 212- by 212-μm fields of view, registered from seven different samples, collected in three independent experiments. Data are presented as means ± 95% confidence intervals (CI). The total number of particles and the number of cells were quantified using the ImageJ Fiji tool 3D Objects Counter, and internalized particles were counted manually (*, $P < 0.05$; ****, $P < 0.0001$; ns, not significant). Ab, antibody.

Next, we predicted the M protein topology *in silico*, and based on these data and previous reports, we concluded that regions spanning aa 25 to 51 and aa 93 to 119 may not be involved in the interactions with HPSGs, as they are localized inside the virion or in transmembrane domains (TMDs) (Fig. 6). This led us to the conclusion that the HSPG binding site is localized in the C-terminal region of aa 153 to 226, predicted to be exposed on the virion surface.

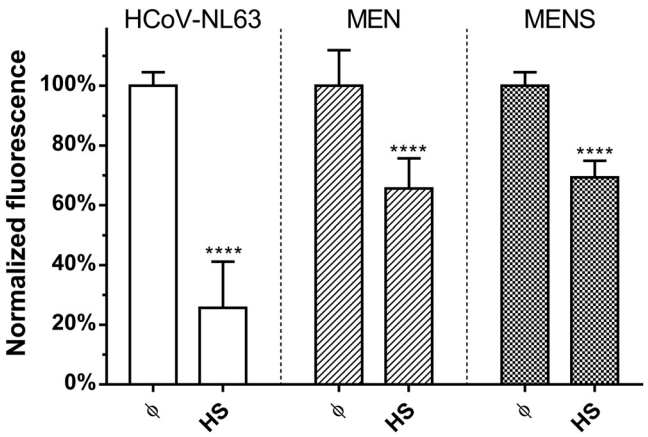

FIG 4 Adhesion of MEN VLPs and MENS VLPs to LLC-Mk2 cells in the presence of heparan sulfate. Flow cytometry analysis was performed on cells incubated with VLPs or HCoV-NL63 in the presence of control PBS (denoted as Ø) or heparan sulfate (denoted as HS). Data are presented as means ± SD. Each bar shows data from a minimum of 5 replicates (****, $P < 0.0001$).

Mapping the heparan sulfate-interacting domain within membrane protein. To further evaluate the interaction between the C-terminal domain of the M protein and HSPGs, we expressed and purified a His-tagged fragment of the M protein consisting of amino acids 153 to 226 (6×His-$M_{153–226}$) in bacteria. To investigate whether the protein adhered to cellular HSPG, we performed an *in situ* enzyme-linked immunosorbent assay (ELISA), with different amounts of the protein added to cells seeded in a microplate. The 6×His-$M_{153–226}$ protein and an equal molar amount of 6×His-N HKU1, as a control, were serially diluted and incubated with LLC-Mk2 cells. A signal developed using an anti-His-horseradish peroxidase (HRP) antibody was detected only with the 6×His-$M_{153–226}$ protein and was proportional to its concentration (Fig. 7A). Importantly, when the 6×His-$M_{153–226}$ protein was preincubated with soluble HS, the interaction with

No.	seq. pos.	peptide sequence	No.	seq. pos.	peptide sequence	No.	seq. pos.	peptide sequence	No.	seq. pos.	peptide sequence
1	1	MSNSSVPLLEVYVHL	15	57	PLVLALSIFDCFVNF	29	113	NPETNAIISLQVYGH	43	169	VIVATPSTTIVCDRV
2	5	SVPLLEVYVHLRNWN	16	61	ALSIFDCFVNFNVDW	30	117	NAIISLQVYGHNYYL	44	173	TPSTTIVCDRVGRSV
3	9	LEVYVHLRNWNFSWN	17	65	FDCFVNFNVDWVFFG	31	121	SLQVYGHNYYLPVMA	45	177	TIVCDRVGRSVNETS
4	13	VHLRNWNFSWNLILT	18	69	VNFNVDWVFFGFSIL	32	125	YGHNYYLPVMAAPTG	46	181	DRVGRSVNETSQTGW
5	17	NWNFSWNLILTLFIV	19	73	VDWVFFGFSILMSII	33	129	YYLPVMAAPTGVTLT	47	185	RSVNETSQTGWAFYV
6	21	SWNLILTLFIVVLQY	20	77	FFGFSILMSIITLCL	34	133	VMAAPTGVTLTLLSG	48	189	ETSQTGWAFYVRAKH
7	25	ILTLFIVVLQYGHYK	21	81	SILMSIITLCLWVMY	35	137	PTGVTLTLLSGVLLV	49	193	TGWAFYVRAKHGDFS
8	29	FIVVLQYGHYKYSRL	22	85	SIITLCLWVMYFVNS	36	141	TLTLLSGVLLVDGHK	50	197	FYVRAKHGDFSGVAS
9	33	LQYGHYKYSRLLYGL	23	89	LCLWVMYFVNSFRLW	37	145	LSGVLLVDGHKIATR	51	201	AKHGDFSGVASQEGV
10	37	HYKYSRLLYGLKMSV	24	93	VMYFVNSFRLWRRVK	38	149	LLVDGHKIATRVQVG	52	205	DFSGVASQEGVLSER
11	41	SRLLYGLKMSVLWCL	25	97	VNSFRLWRRVKTFWA	39	153	GHKIATRVQVGQLPK	53	209	VASQEGVLSEREKLL
12	45	YGLKMSVLWCLWPLV	26	101	RLWRRVKTFWAFNPE	40	157	ATRVQVGQLPKYVIV	54	213	QEGVLSEREKLLHLI
13	49	MSVLWCLWPLVLALS	27	105	RVKTFWAFNPETNAI	41	161	QVGQLPKYVIVATPS			
14	53	WCLWPLVLALSIFDC	28	109	FWAFNPETNAIISLQ	42	165	LPKYVIVATPSTTIV			

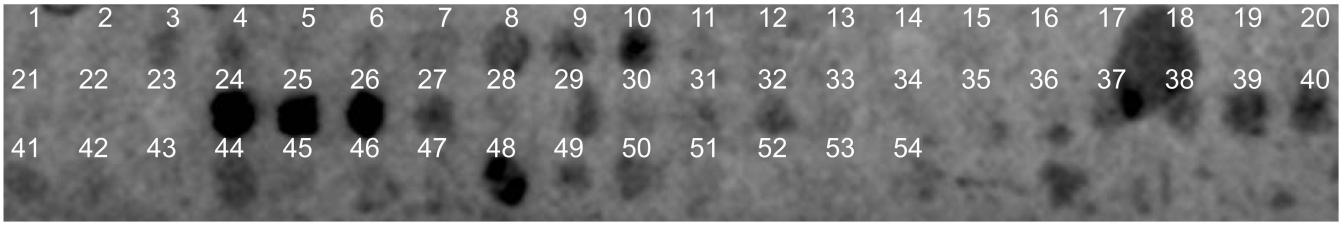

FIG 5 Peptide array. Synthetic peptides covering the M protein sequence were immobilized on a cellulose membrane and incubated with biotinylated heparin. The interaction was detected as a chemiluminescence signal with HRP-conjugated streptavidin. Numbers on the cellulose membrane (bottom) correspond to peptide numbers listed at the top.

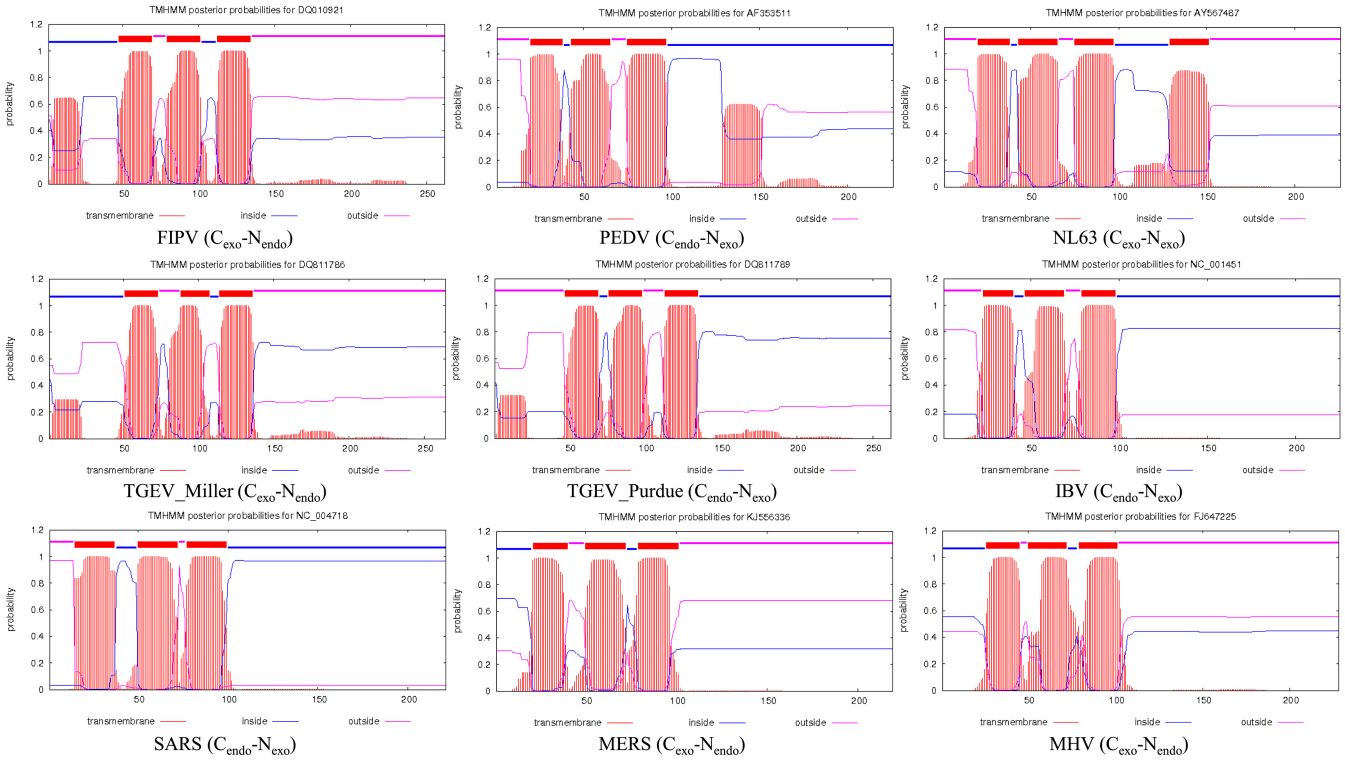

FIG 6 Theoretical topology prediction of selected coronaviruses. Graphs were generated with the TMHMM server online tool (www.cbs.dtu.dk/services/TMHMM). GenBank accession numbers of analyzed sequences are AY567487 for human coronavirus NL63; DQ010921 for feline coronavirus strain FIPV 79-1146; AF353511 for porcine epidemic diarrhea virus strain CV777; DQ811789 for virulent TGEV Purdue; DQ811786 for TGEV Miller M60; NC_001451 for avian infectious bronchitis virus; NC_004718, NC_028845, NC_028858, NC_028866, NC_028873, and NC_028884 for SARS coronavirus; KJ556336 for Middle East respiratory syndrome coronavirus isolate Jeddah_1_2013; and FJ647225 for murine coronavirus inf-MHV-A59.

LLC-Mk2 cells was diminished (Fig. 7B), suggesting that the putative epitope is localized within the region from aa 153 to 226 of the M protein.

Inhibition of virus adhesion to the cell surface by anti-M antibody binding. To further validate the notion that HCoV-NL63 employs the M protein to bind to the cell, we performed a "pseudoneutralization" assay using a polyclonal anti-M rabbit serum, obtained after immunizing rabbits with peptides corresponding to aa 181 to 195 and aa 211 to 226 of the M protein. Purified MEN and MENS VLPs and HCoV-NL63 were

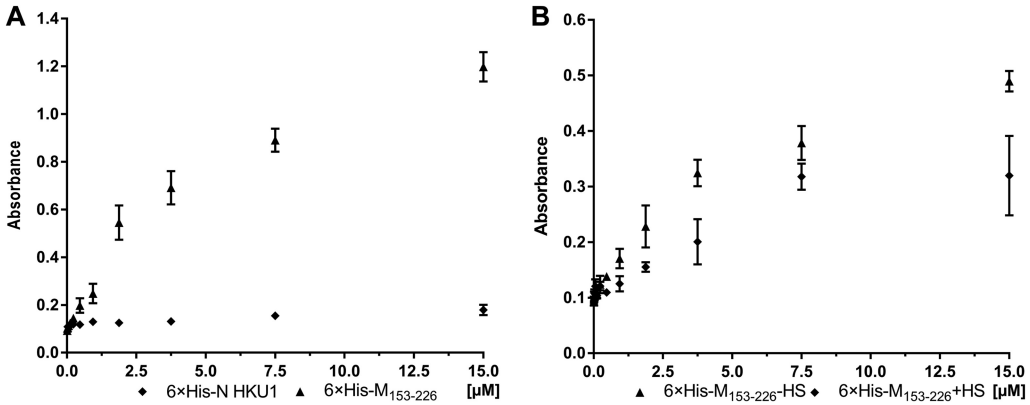

FIG 7 *In situ* ELISA. The 6×His-$M_{153–226}$ protein interacts with LLC-Mk2 cells. Cells were incubated with 6×His-$M_{153–226}$ protein and 6×His-N HKU1 protein, as a control (A), or with HS-preincubated 6×His-$M_{153–226}$ protein (B). Protein adhesion to cells was detected with anti-His-HRP antibody and measured in a spectrophotometer. All measurements were done in triplicates, and the background signal was subtracted from the calculated mean values. The results shown are representative of data from three independent experiments.

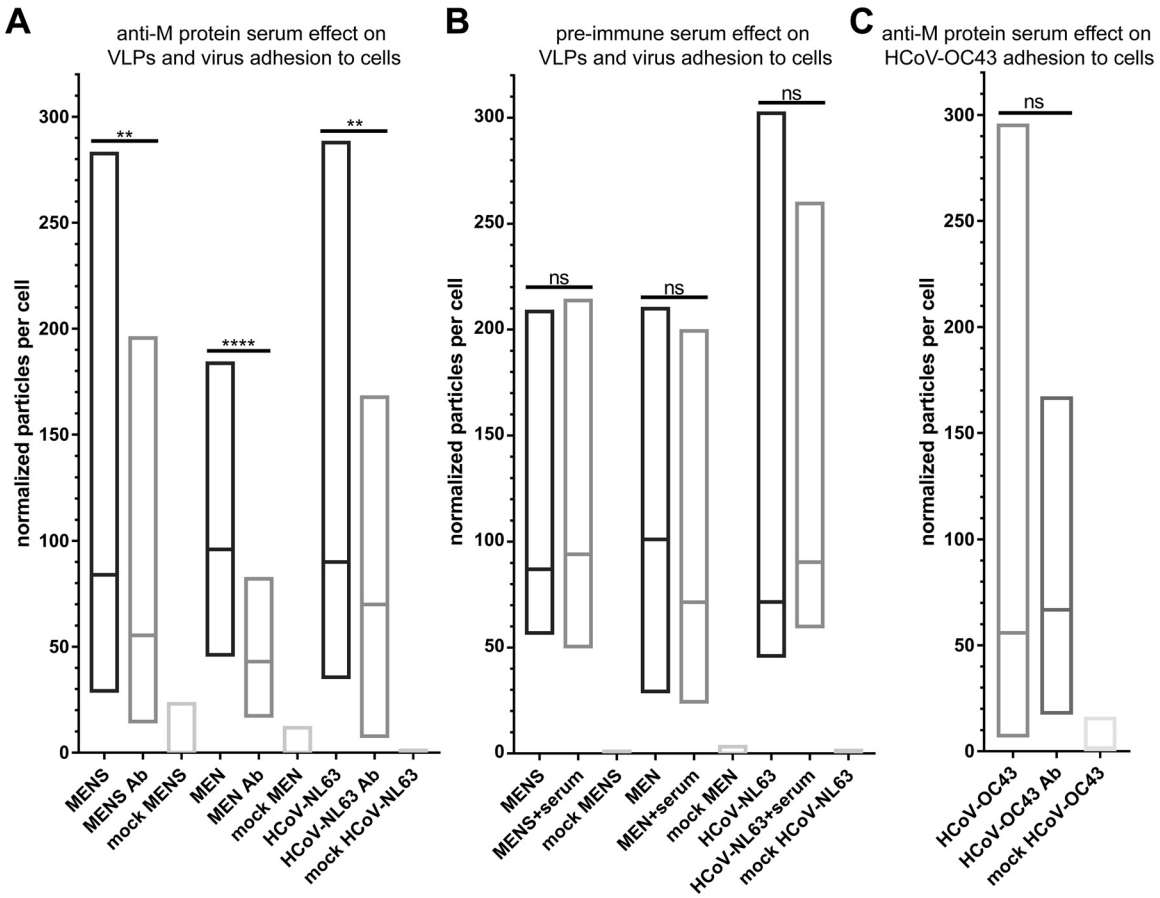

FIG 8 VLP and HCoV-NL63 pseudoneutralization assay. (A and B) LLC-Mk2 cells were inoculated with MEN or MENS VLPs or HCoV-NL63 preincubated with anti-M serum, denoted "Ab" (A), or the respective preimmune serum (B). (C) The specificity of anti-M serum was examined by testing its effect on HCoV-OC43 adhesion to HRT-18G cells. Cells fixed and stained with anti-N monoclonal antibody were visualized using confocal microscopy. The number of particles and number of cells were quantified using the ImageJ Fiji 3D Objects Counter tool. The number of particles per cell is presented as a minimum-maximum graph with a line set at the median value. Each bar shows data from a minimum of 24 212- by 212-μm fields of view, registered from three different samples (**, $P < 0.01$; ****, $P < 0.0001$).

preincubated with the serum and used to inoculate LLC-Mk2 cells. Adhesion of VLPs or HCoV-NL63 to cells was evaluated by confocal microscopy. As shown in Fig. 8, VLPs and HCoV-NL63 adhere to the cells in the control sample, but this interaction was impaired in the presence of the anti-M serum.

DISCUSSION

Cell infection is a complex process that involves viral attachment, which leads to viral enrichment on the cell surface and subsequent internalization. While initial binding is usually nonspecific and mediated by ubiquitous molecules, such as sugars or glycoconjugates (glycoproteins, glycolipids, and proteoglycans), the second step requires a highly specific interaction with the entry receptors, often involving their proteolytic processing. In some viruses, a single protein is responsible for both steps of this interaction, whereas in other viruses (i.e., paramyxoviruses), different structural elements of the virion are employed for the attachment to and fusion with the cellular membrane (26). This sophisticated interplay of distinct receptor entities and their sequential engagement increase viral avidity and coordination in time for key events for efficient cellular uptake.

For coronaviruses, it is generally believed that S protein is responsible for both virion attachment and internalization (reviewed in references 27 and 28). This large (~150-kDa) glycoprotein consists of three segments: an ectodomain, a transmembrane anchor, and a short endodomain. The ectodomain can be further divided into S1 and S2

subunits, although not all coronaviruses undergo enzymatic cleavage of the S ectodomain (29). Different experimental approaches demonstrating that the S1 domain encompasses one or more receptor binding sites (RBSs), located at its C terminus, have been reported for almost all studied CoVs. While the C-terminal part of the S1 domain (S1-CTD) is highly divergent and responsible for the interaction with entry receptors, the more conserved N-terminal region of S1 (S1-NTD) is thought to function as a ligand for the initial attachment factors. Indeed, it was demonstrated that the S1-NTDs of several coronaviruses bind carbohydrates. Examples include the alphacoronavirus (TGEV), betacoronavirus (HCoV-HKU1 and BCoV), and gammacoronavirus (IBV) genera (30–33). In contrast, the S2 domain presumably participates in the fusion of the cellular membrane with the viral envelope (34). This was confirmed for a number of coronaviruses, including HCoV-229E (35), SARS-CoV (36), MHV (37), and HCoV-NL63 (38).

The structure of the HCoV-NL63 S protein and its role in viral infection were previously described (3, 39–42). The receptor binding domain (RBD) within the S1 subunit and the heptad repeat region within the S2 subunit were mapped (38). Some authors speculate that S1 also contains a domain responsible for binding to the attachment receptors on the cell surface, which triggers binding with ACE2 (27, 41). Of note, it has been shown that purified full-length S protein of HCoV-NL63 exhibits surprisingly low-affinity binding to its putative receptor (43). At the same time, there is evidence that the RBD of the HCoV-NL63 S protein binds ACE2 with a higher affinity than its full-length counterpart and with efficiency comparable to that of S1 of SARS-CoV (40, 41, 44). These observations raise questions about the existence of an additional, S-independent stimulus prerequisite for this interaction.

In the present study, we provide evidence that the M protein may be responsible for the interaction of the virus with cellular HSPG. For this, we have used previously developed VLPs, produced in insect cells, which enable efficient and scalable expression of complex macromolecular structures. First, using confocal microscopy, we showed that adhesion to the cell surface was not abrogated in VLPs missing the S protein. Moreover, blocking the VLP-ACE2 interaction with specific antibodies did not affect adhesion. Next, using flow cytometry, we confirmed that adhesion is mediated by HSPG, since soluble HS blocks the interaction. To identify the ligand involved in this interaction, we decided to first screen the M protein for the presence of putative heparin binding domains. Using a simple peptide array overlay, we identified three regions that may potentially be responsible for such an interaction. The experimental data were consistent with the notion that these regions are rich in positively charged amino acids, lysine, and arginine (45, 46). Subsequently, we verified this result using the predicted topology of the M protein and literature data. Only one site was predicted to localize on the virion surface, and consequently, we assumed that this particular site is responsible for the interaction. This assumption was then proven by an *in situ* ELISA, which demonstrated that the region from aa 153 to 226 of the M protein binds to cellular HSPG.

Of note, topology prediction algorithms detected four transmembrane domains (TMDs) within the M protein, which is somewhat atypical for coronaviruses (Fig. 6). The C terminus of the M protein is essential for the M-M, M-N, and M-S interactions, and it is thought to be hidden within the virion envelope (6, 47–51). However, the exact region of the M protein responsible for these interactions has not been defined for most coronaviruses. Recently, it was suggested that this interaction might rely on structural motifs consisting of several residues dispersed throughout the protein (52). Furthermore, we have previously demonstrated that a C-terminally tagged M protein is assembly competent for VLP formation, which supports the four-TMD model of the M protein and the resulting N_{exo}-C_{exo} topology. This conclusion was validated by the observation that HCoV-NL63 and NL63 VLP adhesion is hampered by an antibody raised against two peptides corresponding to the distal part of the M protein. Interestingly, this observation was consistent with works of Enjuanes and colleagues (53, 54), who demonstrated a similar M protein topology of TGEV CoV belonging to the same genus (alphacoronavirus) as HCoV-NL63. Hence, we propose that such a unique organization

of the NL63-HCoV M protein might be one explanation for its engagement in HCoV-NL63 infection.

It has to be mentioned that some coronaviruses acquire the ability to bind HSPG in the course of cell culture adaptation, as described for MHV and IBV (13, 55–57). To exclude this possibility, we compared the M protein sequence used in the present study (Amsterdam I strain) with those of clinical isolates, and no differences in this region were identified (not shown). We believe that the engagement of the M protein in cell attachment is hence a natural characteristic of HCoV-NL63.

The involvement of proteins other than the S protein in carbohydrate binding by coronaviruses has been previously described. For instance, HE of an MHV strain binds cellular sialic acids (58). HE also appears to mediate the attachment of BCoV and HCoV-OC43 to the cell surface (33, 59, 60). More generally, the involvement of multiple capsid proteins was described for a number of viruses, i.e., influenza virus (paramyxoviruses) or herpesviruses (reviewed in references 61 and 62). It is also worth mentioning that the presented results do not preclude the participation of S protein in the recognition of cellular HSPG during HCoV-NL63 infection.

The observations presented here provide new insight into the understanding of cell receptors and their interplay with the viral ligands during HCoV-NL63 infection. Considering the role of the M protein, one could suggest novel strategies for inhibiting or preventing infection by this and potentially other coronaviruses. Specifically, some experimental anticoronaviral vaccines that induce anti-S protein humoral responses cause serious adverse effects, probably related to an antibody-dependent enhancement mechanism (63–65). In this context, vaccines, immunotherapeutics, or antivirals developed to inhibit the interaction between the M protein and cellular HSPG may offer an interesting alternative.

MATERIALS AND METHODS

Cell lines. Sf9 (*Spodoptera frugiperda*; ATCC CRL-1711) and HF (High Five) (*Trichoplusia ni*; ATCC CRL-7701) cells were cultured in ESF medium (Expression Systems, CA, USA) supplemented with 2% FBS (fetal bovine serum; Thermo Fisher Scientific, Poland), 100 μg/ml streptomycin, 100 IU/ml penicillin, 10 μg/ml gentamicin, and 0.25 μg/ml amphotericin B. The culture was maintained in a humidified incubator at 27°C. Sf9 cells were used for baculovirus (BV) generation and amplification, while HF cells were used for recombinant protein expression.

LLC-Mk2 cells (*Macaca mulatta* kidney epithelial cells; ATCC CCL-7) were maintained in minimal essential medium (MEM) (2 parts Hanks' MEM and 1 part Earle's MEM; Thermo Fisher Scientific, Poland) supplemented with 3% FBS, 100 μg/ml streptomycin, 100 IU/ml penicillin, and 5 μg/ml ciprofloxacin. The culture was maintained at 37°C under 5% CO_2.

VLP production. VLPs composed of membrane (M), envelope (E), and spike (S) proteins of HCoV-NL63 were produced as described previously (22), but nucleocapsid (N) protein was additionally included for this work. For this, the N gene was subcloned from pET Duet (23) to pFastBac Dual, under the control of the polyhedrin promoter. Recombinant baculoviruses (rBVs) were generated using the Bac-to-Bac system (Thermo Fisher Scientific, Poland) and titrated using a plaque assay. Subsequently, HF cells were coinfected with (M+E) bicistronic rBV, N monocistronic rBV, and S monocistronic rBV at a multiplicity of infection (MOI) of 4 and cultured for 72 h. Secreted VLPs were then harvested by centrifugation (5,000 $\times$ *g* for 30 min).

For purification of VLPs, the harvested culture medium was diluted (1:1) with binding buffer (20 mM K_2HPO_4-KH_2PO_4 [pH 6.2], 70 mM NaCl) and loaded onto a 5-ml heparin HT column (GE Healthcare, Poland) using an Äkta fast-performance liquid chromatography (FPLC) system (Äkta, Sweden). Before purification, the column was equilibrated with binding buffer. Proteins were eluted with a linear NaCl gradient (50 mM to 2 M NaCl in binding buffer), and collected peak fractions were analyzed using SDS-PAGE and Western blotting.

SDS-PAGE and Western blotting. Insect cells or culture media were harvested, resuspended in denaturing buffer to final concentrations of 1.5% SDS and 2.5% β-mercaptoethanol, and resolved by Laemmli SDS-PAGE using 4-to-20% gradient precast gels (Bio-Rad, Poland). A PageRuler Prestained Plus protein ladder (Thermo Fisher Scientific, Poland) was used in this study as a protein size marker. Gels were stained with Coomassie brilliant blue or subjected to electrotransfer in buffer containing 25 mM Tris, 192 mM glycine, and 20% methanol onto an activated polyvinylidene difluoride (PVDF) membrane. Following transfer, the membrane was blocked with 5% skim milk in Tris-buffered saline supplemented with 0.05% Tween 20 (TBS-T), followed by 1.5 h of incubation with rabbit polyclonal anti-M serum (1:15,000; kindly provided by Lia van der Hoek and generated by rabbit immunization with peptides spanning aa 180 to 195 and aa 212 to 226 of the M protein), mouse monoclonal anti-N antibody (1:1,000; Ingenansa, Spain), and mouse polyclonal anti-S serum (1:250; Eurogentec, Belgium) and 1 h of incubation with anti-rabbit (1:20,000; Dako, Denmark) and anti-mouse (1:20,000; Dako, Denmark) secondary antibodies conjugated with horseradish peroxidase (HRP), respectively. The signal was developed using the

Immobilon Western chemiluminescent HRP substrate (Millipore, Poland) and visualized by exposing the membrane to an X-ray film (Thermo Fisher Scientific, Poland).

Confocal microscopy. For assessment of protein colocalization in insect cells, HF cells were grown in 6-well culture plates on glass coverslips coated with 0.01% poly-L-ornithine (Sigma-Aldrich, Poland). Cells were infected with rBVs at an MOI of 1, fixed at 48 h postinfection with 4% formaldehyde, permeabilized with 0.2% Triton X-100 in phosphate-buffered saline (PBS), and blocked for 1 h, at room temperature with 5% bovine serum albumin (BSA) in PBS. Expression of M and N proteins was detected with rabbit polyclonal anti-M serum (the same as described above; 1:1,000) and mouse monoclonal anti-N antibody (the same as described above; 1:2,000), respectively, followed by detection with Alexa fluorophore secondary antibodies at a 1:400 dilution (Santa Cruz Biotechnology, USA). Cell nuclei were stained with DAPI (4′,6′-diamidino-2-phenylindole) (0.1 g/ml in PBS; Sigma-Aldrich, Poland). Coverslips were mounted on glass slides with Prolong diamond antifade mountant (Sigma-Aldrich, Poland).

For transduction and adhesion analyses of VLPs, LLC-Mk2 cells were grown to 80% confluence for 48 h in 6-well culture plates on glass coverslips. Cells were then washed with ice-cold PBS and inoculated with 1 ml of purified VLPs. Next, LLC-Mk2 cells were incubated for 2 h at 4°C and subsequently for 90 min at 32°C under 5% CO_2 and further washed three times with PBS. Subsequently, cells were fixed, permeabilized, and stained with anti-M polyclonal serum, as described above. Additionally, actin filaments were visualized with phalloidin conjugated with Alexa 647 (0.132 μM; Sigma-Aldrich, Poland).

To verify the role of the ACE2 protein during VLP entry, LLC-Mk2 cells were incubated with anti-ACE2 polyclonal antibodies (catalog number AF933; R&D Systems) or an appropriate isotype control antibody (catalog number GTX35039; GeneTex) for 1 h at 37°C (5 μg/ml). The anti-ACE2 antibody concentration was determined based on HCoV-NL63 neutralization experiments in LLC-Mk2 cells (not shown). Furthermore, cells were overlaid with purified MEN or MENS VLPs and incubated for 2 h at 4°C and subsequently for 90 min at 32°C under 5% CO_2 in the presence of antibodies. Next, cells were washed three times with PBS, fixed, permeabilized, and stained with anti-M polyclonal serum, as described above.

Fluorescent images were acquired using a Zeiss LSM 710 confocal microscope (Carl Zeiss Microscopy GmbH), deconvolved using AutoQuant X3 software, and processed in ImageJ Fiji (National Institutes of Health, Bethesda, MD, USA) (66).

The number of particles and number of cells were quantified using the built-in ImageJ Fiji tool "3D Objects Counter." The numbers of internalized particles were counted manually from orthogonal views. For this study, the actin cortex was assumed to indicate the cell surface.

Electron microscopy. Samples were prepared as described previously (22). Briefly, purified VLPs were fixed in Karnovsky solution and loaded onto copper grids coated with a support film (Formvar 15/95E; Sigma-Aldrich, St. Louis, MO, USA). After drying, the material was stained with uranyl acetate (Polyscience, Inc., Warrington, PA, USA) and lead citrate (Sigma-Aldrich, St. Louis, MO, USA). Subsequently, the grids were washed with water and dried in air at room temperature. Ultrastructural observations were performed by using a Hitachi H500 transmission electron microscope at an accelerating voltage of 75 kV.

Flow cytometry. To evaluate adhesion of VLPs to LLC-Mk2 cells, cells were grown for 48 h to reach 100% confluence in 6-well culture plates on glass coverslips. Cells were washed twice with PBS and incubated with purified VLPs, iodixanol-concentrated HCoV-NL63 (12, 67), mock supplemented with heparan sulfate (HS) (1 mg/ml; Sigma-Aldrich, Poland), or PBS for 4 h at 4°C. The cells were then washed three times with PBS, fixed with 4% paraformaldehyde, permeabilized with 0.1% Triton X-100 in PBS, and incubated overnight in 5% bovine serum albumin and 0.5% Tween 20 in PBS. To examine HCoV-NL63 or VLP adhesion, cells were incubated for 2 h at room temperature with a mouse monoclonal anti-N antibody (the same as described above; 1:1,000 in 2.5% BSA with 0.5% Tween 20 in PBS), followed by 1 h of incubation with an Alexa Fluor 488-labeled goat anti-mouse antibody (1:400). Cells were then washed, mechanically detached from the glass coverslips, resuspended in PBS, and analyzed by flow cytometry (FACSCalibur; Becton, Dickinson). Data were processed using CellQuest software (Becton, Dickinson) and FlowJo V10.

Expression of the C-terminal domain of the M protein. The region coding for the C-terminal fragment (aa 153 to 226) of the M protein was PCR amplified (5′ primer CCA gga tcc gGA TGG CCA TAA GAT TGC TAC TCG TG and 3′ primer GCA ctc gag TTA GAT TAA ATG AAG CAA CTT), digested with BamHI and XhoI enzymes (Thermo Fisher Scientific, Poland), gel purified, and cloned into the pET Duet plasmid in a manner to include the 6×His tag in frame at the N terminus. The sequence (6×His-$M_{153–226}$) was verified by sequencing. The *Escherichia coli* BL21 strain was transformed with the recombinant plasmid and precultured overnight at 37°C. LB medium (1 liter; BioShop-LabEmpire, Poland) was inoculated with the preculture, induced with isopropyl-β-D-thiogalactopyranoside (IPTG) (0.5 mM; BioShop-LabEmpire, Poland) at an optical density of 0.6, and harvested at 4 h postinduction. Bacterial cell pellets were subsequently resuspended in 50 ml of lysis buffer (50 mM Tris [pH 7.5], 5 mM urea, 250 mM NaCl, 5 mM dithiothreitol [DTT], 1 mM EDTA, 1% Triton X-100) and subjected to 2 cycles of Cell Disruptor (Constant Systems, UK) operation at 25 lb/in^2. Lysates were then centrifuged (40 min at 5,000 × *g*), and the supernatant was diluted (1:1) with immobilized-metal affinity chromatography (IMAC) binding buffer (20 mM K_2HPO_4-KH_2PO_4 [pH 7.4], 500 mM NaCl, 20 mM imidazole). Diluted supernatants were loaded onto a 1-ml IMAC column (GE Healthcare, Poland) charged with Ni^{2+} and connected to an Äkta FPLC system (Äkta, Sweden) and preequilibrated with binding buffer. Proteins were eluted with 500 mM imidazole in IMAC binding buffer. Collected peak fractions were pooled and fractionated again to remove imidazole and excess NaCl. For this purpose, a 26/10 desalting column (GE Healthcare, Poland) (preequilibrated with 20 mM Na_2HPO_4-NaH_2PO_4 [pH 7.7], 250 mM NaCl, and 5% glycerol) was used. Purified 6×His-$M_{153–226}$ protein was analyzed by SDS-PAGE and Western blotting.

***In situ* ELISA.** LLC-Mk2 cells were seeded into a 96-well plate 48 h prior to the assay and incubated at 37°C under 5% CO_2. Purified 6×His-$M_{153–226}$ protein (initial concentration of 0.15 mg/ml) was 2-fold serially diluted with PBS and transferred to a plate with confluent LLC-Mk2 cells. As a control, 6×His-N HKU1 was prepared in the same manner and added to the cells at the same molar ratio. After 2 h of incubation at 32°C under 5% CO_2, the culture plate was inverted to remove unbound material, and cells were washed 4 times with PBS. Next, unspecific binding sites on the plate were blocked with 5% bovine serum albumin in PBS for 1 h, and subsequently, samples were incubated for 90 min with anti-His antibody conjugated with HRP (1:10,000; Sigma, Poland). The signal was visualized with the 3,3′,5,5′-tetramethylbenzidine (TMB) substrate (OptiEIA; Becton, Dickinson, USA), and the reaction was stopped with 1 M HCl. The absorbance was measured at a wavelength (λ) of 450 nm using a Tecan Infinite 200 Pro microplate reader. All measurements were performed in triplicate, and the background signal (from control wells) was subtracted. Another *in situ* ELISA was performed to evaluate 6×His-$M_{153–226}$ protein binding to LLC-Mk2 cells in the presence or absence of soluble HS. Briefly, 6×His-$M_{153–226}$ protein was preincubated for 30 min at room temperature with HS (1 mg/ml in PBS) and transferred to a plate with confluent LLC-Mk2 cells. As a control, 6×His-$M_{153–226}$ (diluted in the same manner) was added to cells. After 2 h of incubation at 32°C under 5% CO_2, the culture plate was processed as described above.

Peptide array. A cellulose membrane displaying 54 immobilized peptides covering the whole membrane protein (15 amino acids each, with a sliding window with a 4-aa step) was designed and purchased from JPT Peptides GmbH (Germany). The cellulose membrane was activated in methanol for 5 min, washed three times with TBS-T, and blocked for 2 h with 2.5% skimmed milk (in TBS-T). Next, the membrane was incubated for 3 h with 10 ml of heparin conjugated with biotin (10 μg/ml in PBS; Sigma-Aldrich, Poland), washed 4 times in TBS-T, and incubated for 2 h with 5 ml of streptavidin-HRP (2 μg/ml in PBS; Sigma-Aldrich, Poland). Following extensive washing (4 times) with TBS-T, the signal was developed using the Immobilon Western chemiluminescent HRP substrate (Millipore, Poland) and visualized by exposing the membrane to an X-ray film (Thermo Fisher Scientific, Poland).

Topology prediction. The TMHMM server, v. 2.0, for prediction of transmembrane helices in proteins (68) was used to evaluate M protein topology.

Pseudoneutralization assay. To verify if anti-M antibody inhibits binding to target cells, purified MEN and MENS VLPs and iodixanol-concentrated HCoV-NL63 were incubated for 1 h at room temperature with an equal volume of rabbit polyclonal anti-M serum at 1:10 or PBS. Next, samples were added to LLC-Mk2 cells seeded on glass coverslips 48 h earlier and grown to 80% confluence and washed with PBS directly before the experiment. After 4 h of incubation at 4°C, cells were washed three times with PBS, fixed, and stained with anti-N antibody for confocal microscopy analysis, as described above. As a control, an identical experiment was conducted with preimmune rabbit serum. Additionally, the effect of anti-M serum on HCoV-OC43 adhesion to HRT-18G cells was examined in a corresponding experiment.

The number of particles and number of cells were quantified using the ImageJ Fiji 3D Objects Counter tool.

Statistical analysis. All data were tested for normality using a Shapiro-Wilk test and a Mann-Whitney test (for pseudoneutralization assays), a Kruskal-Wallis test with Dunn's multiple-comparison test (for the anti-ACE2 antibody effect on VLP adhesion to cells), or one-way analysis of variance (ANOVA) with a Dunnett multiple-comparison test (for the HS effect on VLPs adhesion to cells). *P* values of <0.05 were considered significant. All graphs were prepared using GraphPad Prism 7.

Accession number(s). The nucleotide sequences of the N, M, E, and S genes appear in the GenBank database under accession numbers NC_005831.2, MH050812, MH050811, and MH050813, respectively.

ACKNOWLEDGMENTS

This work was supported by the National Science Center in Poland within an FUGA grant (UMO-2013/08/S/NZ6/00730) and a Sonata Bis grant (UMO-2012/07/E/NZ6/01712). Part of the work was also supported by the National Centre for Research and Development, Poland (Lider/27/55/L-2/10/2011). K.P. acknowledges networking contribution by COST Action CM1407, Challenging Organic Syntheses Inspired by Nature—from Natural Products Chemistry to Drug Discovery. The Faculty of Biochemistry, Biophysics, and Biotechnology of the Jagiellonian University is a beneficiary of structural funds from the European Union (grant number POIG.02.01.00-12-064/08, Molecular Biotechnology for Health). The Faculty of Biochemistry, Biophysics, and Biotechnology of the Jagiellonian University is a partner of the Leading National Research Center supported by the Ministry of Science and Higher Education of the Republic of Poland.

REFERENCES

1. Delmas B, Gelfi J, L'Haridon R, Vogel LK, Sjöström H, Norén O, Laude H. 1992. Aminopeptidase N is a major receptor for the entero-pathogenic coronavirus TGEV. Nature 357:417–420. https://doi.org/10.1038/357417a0.
2. Tresnan DB, Levis R, Holmes KV. 1996. Feline aminopeptidase N serves as a receptor for feline, canine, porcine, and human coronaviruses in serogroup I. J Virol 70:8669–8674.
3. Hofmann H, Pyrc K, van der Hoek L, Geier M, Berkhout B, Pöhlmann S. 2005. Human coronavirus NL63 employs the severe acute respiratory syndrome

coronavirus receptor for cellular entry. Proc Natl Acad Sci U S A 102:7988–7993. https://doi.org/10.1073/pnas.0409465102.
4. Li W, Moore MJ, Vasilieva N, Sui J, Wong SK, Berne MA, Somasundaran M, Sullivan JL, Luzuriaga K, Greenough TC, Choe H, Farzan M. 2003. Angiotensin-converting enzyme 2 is a functional receptor for the SARS coronavirus. Nature 426:450–454. https://doi.org/10.1038/nature02145.
5. Taguchi F, Hirai-Yuki A. 2012. Mouse hepatitis virus receptor as a determinant of the mouse susceptibility to MHV infection. Front Microbiol 3:68. https://doi.org/10.3389/fmicb.2012.00068.
6. Ujike M, Taguchi F. 2015. Incorporation of spike and membrane glycoproteins into coronavirus virions. Viruses 7:1700–1725. https://doi.org/10.3390/v7041700.
7. Mou H, Raj VS, van Kuppeveld FJ, Rottier PJ, Haagmans BL, Bosch BJ. 2013. The receptor binding domain of the new Middle East respiratory syndrome coronavirus maps to a 231-residue region in the spike protein that efficiently elicits neutralizing antibodies. J Virol 87:9379–9383. https://doi.org/10.1128/JVI.01277-13.
8. Saeki K, Ohtsuka N, Taguchi F. 1997. Identification of spike protein residues of murine coronavirus responsible for receptor-binding activity by use of soluble receptor-resistant mutants. J Virol 71:9024–9031.
9. Collins AR. 1993. HLA class I antigen serves as a receptor for human coronavirus OC43. Immunol Invest 22:95–103. https://doi.org/10.3109/08820139309063393.
10. Hulswit RJ, de Haan CA, Bosch BJ. 2016. Coronavirus spike protein and tropism changes. Adv Virus Res 96:29–57. https://doi.org/10.1016/bs.aivir.2016.08.004.
11. Li F. 2015. Receptor recognition mechanisms of coronaviruses: a decade of structural studies. J Virol 89:1954–1964. https://doi.org/10.1128/JVI.02615-14.
12. Milewska A, Zarebski M, Nowak P, Stozek K, Potempa J, Pyrc K. 2014. Human coronavirus NL63 utilizes heparan sulfate proteoglycans for attachment to target cells. J Virol 88:13221–13230. https://doi.org/10.1128/JVI.02078-14.
13. Watanabe R, Sawicki SG, Taguchi F. 2007. Heparan sulfate is a binding molecule but not a receptor for CEACAM1-independent infection of murine coronavirus. Virology 366:16–22. https://doi.org/10.1016/j.virol.2007.06.034.
14. Lang J, Yang N, Deng J, Liu K, Yang P, Zhang G, Jiang C. 2011. Inhibition of SARS pseudovirus cell entry by lactoferrin binding to heparan sulfate proteoglycans. PLoS One 6:e23710. https://doi.org/10.1371/journal.pone.0023710.
15. Huan CC, Wang Y, Ni B, Wang R, Huang L, Ren XF, Tong GZ, Ding C, Fan HJ, Mao X. 2015. Porcine epidemic diarrhea virus uses cell-surface heparan sulfate as an attachment factor. Arch Virol 160:1621–1628. https://doi.org/10.1007/s00705-015-2408-0.
16. Summerford C, Samulski RJ. 1998. Membrane-associated heparan sulfate proteoglycan is a receptor for adeno-associated virus type 2 virions. J Virol 72:1438–1445.
17. Dechecchi MC, Melotti P, Bonizzato A, Santacatterina M, Chilosi M, Cabrini G. 2001. Heparan sulfate glycosaminoglycans are receptors sufficient to mediate the initial binding of adenovirus types 2 and 5. J Virol 75:8772–8780. https://doi.org/10.1128/jvi.75.18.8772-8780.2001.
18. Shafti-Keramat S, Handisurya A, Kriehuber E, Meneguzzi G, Slupetzky K, Kirnbauer R. 2003. Different heparan sulfate proteoglycans serve as cellular receptors for human papillomaviruses. J Virol 77:13125–13135. https://doi.org/10.1128/JVI.77.24.13125-13135.2003.
19. Shukla D, Spear PG. 2001. Herpesviruses and heparan sulfate: an intimate relationship in aid of viral entry. J Clin Invest 108:503–510. https://doi.org/10.1172/JCI13799.
20. Schäfer G, Blumenthal MJ, Katz AA. 2015. Interaction of human tumor viruses with host cell surface receptors and cell entry. Viruses 7:2592–2617. https://doi.org/10.3390/v7052592.
21. Bartlett AH, Park PW. 2010. Proteoglycans in host-pathogen interactions: molecular mechanisms and therapeutic implications. Expert Rev Mol Med 12:e5. https://doi.org/10.1017/S1462399409001367.
22. Naskalska A, Dabrowska A, Nowak P, Szczepanski A, Jasik K, Milewska A, Ochman M, Zeglen S, Rajfur Z, Pyrc K. 2018. Novel coronavirus-like particles targeting cells lining the respiratory tract. PLoS One 13:e0203489. https://doi.org/10.1371/journal.pone.0203489.
23. Zuwała K, Golda A, Kabala W, Burmistrz M, Zdzalik M, Nowak P, Kedracka-Krok S, Zarebski M, Dobrucki J, Florek D, Zeglen S, Wojarski J, Potempa J, Dubin G, Pyrc K. 2015. The nucleocapsid protein of human coronavirus NL63. PLoS One 10:e0117833. https://doi.org/10.1371/journal.pone.0117833.
24. Fromm JR, Hileman RE, Caldwell EE, Weiler JM, Linhardt RJ. 1997. Pattern and spacing of basic amino acids in heparin binding sites. Arch Biochem Biophys 343:92–100. https://doi.org/10.1006/abbi.1997.0147.
25. Caldwell EE, Nadkarni VD, Fromm JR, Linhardt RJ, Weiler JM. 1996. Importance of specific amino acids in protein binding sites for heparin and heparan sulfate. Int J Biochem Cell Biol 28:203–216. https://doi.org/10.1016/1357-2725(95)00123-9.
26. Knipe DM, Howley PM, Cohen JI, Griffin DE, Lamb RA, Martin MA, Racaniello VR, Roizman B (ed). 2013. Fields virology, 6th ed. Lippincott Williams & Wilkins, Philadelphia, PA.
27. Reguera J, Mudgal G, Santiago C, Casasnovas JM. 2014. A structural view of coronavirus-receptor interactions. Virus Res 194:3–15. https://doi.org/10.1016/j.virusres.2014.10.005.
28. Li F. 2016. Structure, function, and evolution of coronavirus spike proteins. Annu Rev Virol 3:237–261. https://doi.org/10.1146/annurev-virology-110615-042301.
29. Belouzard S, Millet JK, Licitra BN, Whittaker GR. 2012. Mechanisms of coronavirus cell entry mediated by the viral spike protein. Viruses 4:1011–1033. https://doi.org/10.3390/v4061011.
30. Krempl C, Schultze B, Laude H, Herrler G. 1997. Point mutations in the S protein connect the sialic acid binding activity with the enteropathogenicity of transmissible gastroenteritis coronavirus. J Virol 71:3285–3287.
31. Peng G, Xu L, Lin YL, Chen L, Pasquarella JR, Holmes KV, Li F. 2012. Crystal structure of bovine coronavirus spike protein lectin domain. J Biol Chem 287:41931–41938. https://doi.org/10.1074/jbc.M112.418210.
32. Promkuntod N, van Eijndhoven RE, de Vrieze G, Gröne A, Verheije MH. 2014. Mapping of the receptor-binding domain and amino acids critical for attachment in the spike protein of avian coronavirus infectious bronchitis virus. Virology 448:26–32. https://doi.org/10.1016/j.virol.2013.09.018.
33. Huang X, Dong W, Milewska A, Golda A, Qi Y, Zhu QK, Marasco WA, Baric RS, Sims AC, Pyrc K, Li W, Sui J. 2015. Human coronavirus HKU1 spike protein uses O-acetylated sialic acid as an attachment receptor determinant and employs hemagglutinin-esterase protein as a receptor-destroying enzyme. J Virol 89:7202–7213. https://doi.org/10.1128/JVI.00854-15.
34. Gallagher TM, Buchmeier MJ. 2001. Coronavirus spike proteins in viral entry and pathogenesis. Virology 279:371–374. https://doi.org/10.1006/viro.2000.0757.
35. Bonavia A, Zelus BD, Wentworth DE, Talbot PJ, Holmes KV. 2003. Identification of a receptor-binding domain of the spike glycoprotein of human coronavirus HCoV-229E. J Virol 77:2530–2538. https://doi.org/10.1128/JVI.77.4.2530-2538.2003.
36. Bosch BJ, Martina BE, Van Der Zee R, Lepault J, Haijema BJ, Versluis C, Heck AJ, De Groot R, Osterhaus AD, Rottier PJ. 2004. Severe acute respiratory syndrome coronavirus (SARS-CoV) infection inhibition using spike protein heptad repeat-derived peptides. Proc Natl Acad Sci U S A 101:8455–8460. https://doi.org/10.1073/pnas.0400576101.
37. de Haan CA, Te Lintelo E, Li Z, Raaben M, Wurdinger T, Bosch BJ, Rottier PJ. 2006. Cooperative involvement of the S1 and S2 subunits of the murine coronavirus spike protein in receptor binding and extended host range. J Virol 80:10909–10918. https://doi.org/10.1128/JVI.00950-06.
38. Zheng Q, Deng Y, Liu J, van der Hoek L, Berkhout B, Lu M. 2006. Core structure of S2 from the human coronavirus NL63 spike glycoprotein. Biochemistry 45:15205–15215. https://doi.org/10.1021/bi061686w.
39. Wu K, Li W, Peng G, Li F. 2009. Crystal structure of NL63 respiratory coronavirus receptor-binding domain complexed with its human receptor. Proc Natl Acad Sci U S A 106:19970–19974. https://doi.org/10.1073/pnas.0908837106.
40. Lin HX, Feng Y, Tu X, Zhao X, Hsieh CH, Griffin L, Junop M, Zhang C. 2011. Characterization of the spike protein of human coronavirus NL63 in receptor binding and pseudotype virus entry. Virus Res 160:283–293. https://doi.org/10.1016/j.virusres.2011.06.029.
41. Walls AC, Tortorici MA, Frenz B, Snijder J, Li W, Rey FA, DiMaio F, Bosch BJ, Veesler D. 2016. Glycan shield and epitope masking of a coronavirus spike protein observed by cryo-electron microscopy. Nat Struct Mol Biol 23:899–905. https://doi.org/10.1038/nsmb.3293.
42. Pöhlmann S, Gramberg T, Wegele A, Pyrc K, van der Hoek L, Berkhout B, Hofmann H. 2006. Interaction between the spike protein of human coronavirus NL63 and its cellular receptor ACE2. Adv Exp Med Biol 581:281–284. https://doi.org/10.1007/978-0-387-33012-9_47.
43. Glowacka I, Bertram S, Herzog P, Pfefferle S, Steffen I, Muench MO, Simmons G, Hofmann H, Kuri T, Weber F, Eichler J, Drosten C, Pöhlmann S. 2010. Differential downregulation of ACE2 by the spike proteins of

severe acute respiratory syndrome coronavirus and human coronavirus NL63. J Virol 84:1198–1205. https://doi.org/10.1128/JVI.01248-09.
44. Lin HX, Feng Y, Wong G, Wang L, Li B, Zhao X, Li Y, Smaill F, Zhang C. 2008. Identification of residues in the receptor-binding domain (RBD) of the spike protein of human coronavirus NL63 that are critical for the RBD-ACE2 receptor interaction. J Gen Virol 89:1015–1024. https://doi.org/10.1099/vir.0.83331-0.
45. Liu J, Thorp SC. 2002. Cell surface heparan sulfate and its roles in assisting viral infections. Med Res Rev 22:1–25. https://doi.org/10.1002/med.1026.
46. Cardin AD, Weintraub HJ. 1989. Molecular modeling of protein-glycosaminoglycan interactions. Arteriosclerosis 9:21–32. https://doi.org/10.1161/01.ATV.9.1.21.
47. de Haan CA, Smeets M, Vernooij F, Vennema H, Rottier PJ. 1999. Mapping of the coronavirus membrane protein domains involved in interaction with the spike protein. J Virol 73:7441–7452.
48. Arndt AL, Larson BJ, Hogue BG. 2010. A conserved domain in the coronavirus membrane protein tail is important for virus assembly. J Virol 84:11418–11428. https://doi.org/10.1128/JVI.01131-10.
49. McBride CE, Machamer CE. 2010. A single tyrosine in the severe acute respiratory syndrome coronavirus membrane protein cytoplasmic tail is important for efficient interaction with spike protein. J Virol 84:1891–1901. https://doi.org/10.1128/JVI.02458-09.
50. Tseng YT, Chang CH, Wang SM, Huang KJ, Wang CT. 2013. Identifying SARS-CoV membrane protein amino acid residues linked to virus-like particle assembly. PLoS One 8:e64013. https://doi.org/10.1371/journal.pone.0064013.
51. Neuman BW, Kiss G, Kunding AH, Bhella D, Baksh MF, Connelly S, Droese B, Klaus JP, Makino S, Sawicki SG, Siddell SG, Stamou DG, Wilson IA, Kuhn P, Buchmeier MJ. 2011. A structural analysis of M protein in coronavirus assembly and morphology. J Struct Biol 174:11–22. https://doi.org/10.1016/j.jsb.2010.11.021.
52. Kuo L, Hurst-Hess KR, Koetzner CA, Masters PS. 2016. Analyses of coronavirus assembly interactions with interspecies membrane and nucleocapsid protein chimeras. J Virol 90:4357–4368. https://doi.org/10.1128/JVI.03212-15.
53. Escors D, Camafeita E, Ortego J, Laude H, Enjuanes L. 2001. Organization of two transmissible gastroenteritis coronavirus membrane protein topologies within the virion and core. J Virol 75:12228–12240. https://doi.org/10.1128/JVI.75.24.12228-12240.2001.
54. Risco C, Antón IM, Suñé C, Pedregosa AM, Martín-Alonso JM, Parra F, Carrascosa JL, Enjuanes L. 1995. Membrane protein molecules of transmissible gastroenteritis coronavirus also expose the carboxy-terminal region on the external surface of the virion. J Virol 69:5269–5277.
55. de Haan CA, Li Z, te Lintelo E, Bosch BJ, Haijema BJ, Rottier PJ. 2005. Murine coronavirus with an extended host range uses heparan sulfate as an entry receptor. J Virol 79:14451–14456. https://doi.org/10.1128/JVI.79.22.14451-14456.2005.
56. de Haan CA, Haijema BJ, Schellen P, Wichgers Schreur P, te Lintelo E, Vennema H, Rottier PJ. 2008. Cleavage of group 1 coronavirus spike proteins: how furin cleavage is traded off against heparan sulfate binding upon cell culture adaptation. J Virol 82:6078–6083. https://doi.org/10.1128/JVI.00074-08.
57. Madu IG, Chu VC, Lee H, Regan AD, Bauman BE, Whittaker GR. 2007. Heparan sulfate is a selective attachment factor for the avian coronavirus infectious bronchitis virus Beaudette. Avian Dis 51:45–51. https://doi.org/10.1637/0005-2086(2007)051[0045:HSIASA]2.0.CO;2.
58. Langereis MA, van Vliet AL, Boot W, de Groot RJ. 2010. Attachment of mouse hepatitis virus to O-acetylated sialic acid is mediated by hemagglutinin-esterase and not by the spike protein. J Virol 84:8970–8974. https://doi.org/10.1128/JVI.00566-10.
59. de Groot RJ. 2006. Structure, function and evolution of the hemagglutinin-esterase proteins of corona- and toroviruses. Glycoconj J 23:59–72. https://doi.org/10.1007/s10719-006-5438-8.
60. Desforges M, Desjardins J, Zhang C, Talbot PJ. 2013. The acetyl-esterase activity of the hemagglutinin-esterase protein of human coronavirus OC43 strongly enhances the production of infectious virus. J Virol 87:3097–3107. https://doi.org/10.1128/JVI.02699-12.
61. Akhtar J, Shukla D. 2009. Viral entry mechanisms: cellular and viral mediators of herpes simplex virus entry. FEBS J 276:7228–7236. https://doi.org/10.1111/j.1742-4658.2009.07402.x.
62. Skehel JJ, Wiley DC. 2000. Receptor binding and membrane fusion in virus entry: the influenza hemagglutinin. Annu Rev Biochem 69:531–569. https://doi.org/10.1146/annurev.biochem.69.1.531.
63. Czub M, Weingartl H, Czub S, He R, Cao J. 2005. Evaluation of modified vaccinia virus Ankara based recombinant SARS vaccine in ferrets. Vaccine 23:2273–2279. https://doi.org/10.1016/j.vaccine.2005.01.033.
64. Millet JK, Kien F, Cheung CY, Siu YL, Chan WL, Li H, Leung HL, Jaume M, Bruzzone R, Peiris JS, Altmeyer RM, Nal B. 2012. Ezrin interacts with the SARS coronavirus spike protein and restrains infection at the entry stage. PLoS One 7:e49566. https://doi.org/10.1371/journal.pone.0049566.
65. Jaume M, Yip MS, Kam YW, Cheung CY, Kien F, Roberts A, Li PH, Dutry I, Escriou N, Daeron M, Bruzzone R, Subbarao K, Peiris JS, Nal B, Altmeyer R. 2012. SARS CoV subunit vaccine: antibody-mediated neutralisation and enhancement. Hong Kong Med J 18(Suppl 2):31–36.
66. Schindelin J, Arganda-Carreras I, Frise E, Kaynig V, Longair M, Pietzsch T, Preibisch S, Rueden C, Saalfeld S, Schmid B, Tinevez JY, White DJ, Hartenstein V, Eliceiri K, Tomancak P, Cardona A. 2012. Fiji: an open-source platform for biological-image analysis. Nat Methods 9:676–682. https://doi.org/10.1038/nmeth.2019.
67. Milewska A, Nowak P, Owczarek K, Szczepanski A, Zarebski M, Hoang A, Berniak K, Wojarski J, Zeglen S, Baster Z, Rajfur Z, Pyrc K. 2018. Entry of human coronavirus NL63 into the cell. J Virol 92:e01933-17. https://doi.org/10.1128/JVI.01933-17.
68. Krogh A, Larsson B, von Heijne G, Sonnhammer EL. 2001. Predicting transmembrane protein topology with a hidden Markov model: application to complete genomes. J Mol Biol 305:567–580. https://doi.org/10.1006/jmbi.2000.4315.
69. Neuman BW, Buchmeier MJ. 2016. Supramolecular architecture of the coronavirus particle. Adv Virus Res 96:1–27. https://doi.org/10.1016/bs.aivir.2016.08.005.